Experimental investigation on composite panels of cold-formed steel and timber

Citation for published version:
Kyvelou, P, Reynolds, T, Beckett, CTS & Huang, Y 2021, 'Experimental investigation on composite panels of cold-formed steel and timber', *Engineering Structures*, vol. 247, 113186.
https://doi.org/10.1016/j.engstruct.2021.113186

Digital Object Identifier (DOI):
10.1016/j.engstruct.2021.113186

Link:
Link to publication record in Edinburgh Research Explorer

Document Version:
Peer reviewed version

Published In:
Engineering Structures

EXPERIMENTAL INVESTIGATION ON COMPOSITE PANELS OF COLD-FORMED STEEL AND TIMBER

Pinelopi Kyvelou[1], Thomas Reynolds[2], Chris T. S. Beckett[2], Yuner Huang[2*]

[1] School of Engineering, University of Edinburgh, Scotland, UK (Present address: Department of Civil and Environmental Engineering, Faculty of Engineering, Imperial College London, UK)

[2] School of Engineering, University of Edinburgh, Scotland, UK

ABSTRACT

Timber panels and cold-formed steel sheeting are widely used in the construction industry, especially in prefabricated structures, temporary housing and informal settlements. This is because these materials are widely available, can be cut and fixed with hand tools, and their lightweight makes them easy to transport and build with. When used together, there is a potential for composite action developing between the timber panels and the underlying steel sheeting, which is currently ignored in design. A composite panel of oriented strand boards and cold-formed steel sheeting is proposed herein and its overall structural behaviour is experimentally investigated. Based on results obtained from material, push-out and flexural tests, its mechanical properties are determined and the predominant failure modes are highlighted. The feasibility of mobilising composite action between the components of the proposed system is proven and the derived benefits, both in terms of load carrying capacity and stiffness, are quantified. It is demonstrated that harnessing the beneficial influence of composite action can lead to substantial improvements of the overall structural performance of the proposed composite panel, offering the potential to improve significantly the quality of housing in informal developments and rapidly urbanising areas.

KEYWORDS: Cold-formed steel, composite panels, oriented strand boards, push-out tests, self-drilling screws, structural efficiency

* Corresponding author. Tel.: +44 (0) 131 6505 736, Email: Yuner.Huang@ed.ac.uk.

1 INTRODUCTION

Cold-formed steel (CFS) and timber are primary materials in the construction of informal settlements and temporary and emergency housing worldwide. This is because they are widely available, can be cut and fixed with hand tools, and their lightweight makes them easy to transport and erect manually. Structural elements of low mass are beneficial in terms of earthquake resistance due to reduced inertia forces acting on the structure (Chopra, 2020), while resistance to uplift loading due to high wind loads can be ensured through large panels, tied down to the vertical structural components at regular intervals. Ultimately, when panelised construction of low mass is combined with the use of locally available materials, rapid, economical and efficient construction can be achieved.

Previous research has shown that the mobilisation of composite action is feasible within systems comprising CFS members and timber panels, leading to substantial benefits in terms of load carrying capacity and flexural stiffness. Li (2005) conducted physical experiments on composite beams comprising CFS channels and oriented strand board (OSB) panels, which were found to possess increased flexural rigidity, strength, ductility and stability compared to their equivalent non-composite systems. Fratamico *et al*. (2018) and Kyprianou *et al*. (2018) examined the performance of CFS studs braced with OSB panels, while a series of tests was undertaken by Loss and Frangi (2017) to explore the structural response of innovative steel-timber hybrid floor diaphragms. Kyvelou *et al*. (2015; 2017a; 2018) and Karki *et al*. (2021) investigated the structural performance of floors comprising cold-formed steel joists and wood-based panels, with significant structural benefits observed due to the mobilisation of composite action. Henriques *et al*. (2017) conducted experimental and numerical analyses on light steel framing panels connected with OSB panels using screw connectors, with the yielded results showing that OSB can significantly contribute to the lateral stiffness of the light steel framing panels. More recently, Vella *et al*. (2020) explored experimentally improvements to the connection between cold-formed steel and timber components, with the potential enhancements due to mobilisation of composite action in mind, while Navrathnam *et al*. (2021) developed cross laminated timber-cold-formed steel composite beams for floor systems for use in modular building construction.

In this paper, a lightweight composite system comprising cold-formed steel sheeting and timber panels is proposed for the construction of wall and floor systems for low-rise multi-storey buildings within the framework of a rapidly urbanising society (UN Habitat, 2020). The proposed structural system comprises materials that are widely available: CFS sheeting, which is already widely used for roofing and cladding (Schafer, 2011) and OSB panels. The OSB panels, comprising strands of timber and adhesives, can be manufactured using the smaller pieces of wood produced by small-scale agroforestry, therefore yielding economic and environmental benefits (Rahman *et al*., 2008). Furthermore, there is potential for even further benefits to be gained if composite action arises between the employed components of the proposed structural system. A substantial shear connection at the CFS-OSB interface would be required for this scenario to be realised.

The potential of maximising the structural efficiency of the proposed panels by harnessing the beneficial influence of composite action between the system components is explored herein. A series of material and push-out tests, conducted to determine the fundamental response of the employed materials and connectors respectively is presented, while flexural tests undertaken to investigate the overall structural response of the proposed panels, are presented.

This work makes the following contributions to knowledge:

- the structural performance of this simple, low-cost composite panel system is experimentally demonstrated and its structural behaviour is explained

- the accuracy of existing design methods and theoretical models, linking the component behaviour to that of the complete system, is assessed.

2 MATERIALS AND METHODS

When selecting the structural components of the proposed composite panel, the main criterion was the identification of economical, easily available and lightweight materials in order to facilitate rapid assembly on site. Thus, the proposed panel system, shown in Figure 1, comprises CFS sheeting connected to OSB panels at 100 mm intervals along the ribs of the steel sheet. Bugle-head self-drilling drywall screws of 25 mm length were chosen as shear connectors as they can be installed with hand tools and are the most frequently employed type of fastener currently used in industry to connect cold-formed steel and timber products.

2.1 Material tests

2.1.1 Tensile coupon test on cold-formed steel

Tensile coupon testing was conducted to determine the mechanical properties of the cold-formed steel (CFS) sheets of steel grade S280 with wall thickness of 1.2 mm according to EN 10326 (2004). Three tensile coupons were extracted from an untested cold-formed steel sheet, which was from the same batch as the test specimens for the pull-out and flexural tests of this study. The location of the extracted coupon within the steel panel and its dimensions, determined in accordance with BS ISO 6892-1 (2019), are shown in Figure 2. An electro-mechanical universal testing machine (UTM) Instron 4505 with a loading capacity of 100 kN was used to apply tensile loading on the coupon. A calibrated extensometer with a gauge length of 50 mm was mounted onto the specimen to measure the longitudinal strains during testing. Two strain gauges (one on each side of the coupon) were also attached at the middle of the gauge lengths (BS ISO 6892-1, 2019) to measure the strains at the initial loading stage. In line with BS ISO 6892-1 (2019), the employed loading rate was 0.05 mm/min up to yield and 0.4 mm/min after yield and until fracture. The loading process was paused for 2 minutes at the yield plateau and near the ultimate strength, and the load decreased to the curve corresponding to zero loading rate (Huang and Young, 2014). These lower bound values were used to obtain the corresponding stress-strain curves.

2.1.2 Tensile and compressive tests on OSB material

Tensile coupons, extracted from the longitudinal direction of the OSBs, were tested to obtain the mechanical properties under tension. The dimensions of the tested coupons, shown in Figure 3(a), and the employed testing procedure were in line with BS EN 789 (2004) . Two strain gauges with a gauge length of 120 mm were attached at the mid-length of the coupon specimens (one on each side) while steel plates were attached to the coupon ends with bolts to avoid premature end failure due to the clamping force – see Figure 3(b). A constant loading rate of 0.9 mm/min was employed to ensure occurrence of failure within 3-7 minutes (BS EN 789, 2004).

Three compressive tests were also conducted on OSB coupons to obtain the compressive mechanical properties of the OSB material. The coupons were fabricated according to BS EN 789 (2004), as shown in Figure 4. Test pieces of 310 mm in the longitudinal direction and 220 mm in the transverse direction were extracted from the OSB panels and cut to three equal pieces, which were subsequently glued together with epoxy resin (LOCTITE Hysol EA 9466) – see Figure 4. The coupons were tested in accordance with BS EN 789 (2004) and a linear variable displacement transducer (LVDT) was employed to measure displacements during testing.

2.2 Push-out tests

Push-out tests were carried out to investigate the load-slip response of the shear connectors. Each specimen comprised two OSB panels, one on each side of a CFS panel, connected with self-drilling screws at a constant spacing of 100 mm along the panel ridgelines (to match the connections used in the flexural specimens); a typical specimen is shown in Figure 5. In line with EN 383 (2007), the specimens were subjected to an initial loading cycle up to 40% of the ultimate load carrying capacity P_u, then the load was decreased to 10% of P_u, and then increased again, up to failure. Note that for the first specimen, the unloading and re-loading cycles were omitted, as the ultimate capacity of the system P_u was not yet known. A constant loading rate of 2 mm/min was employed throughout testing to ensure failure at approximately 5 minutes. Rigid steel plates were used at the top and bottom of the specimens, as shown in Figure 5(a), to prevent premature local failure at the end points and ensure an even load distribution. A linear variable displacement transducer (LVDT), attached to the OSB board and pointing at the spreader plate under the loading actuator, was used to measure the relative displacement (slip) at the OSB-CFS interface during testing.

2.3 Flexural tests

Following completion of the push-out tests, flexural tests on full-scale panels were performed to examine the overall structural behaviour of the proposed composite system. Two different composite panels were tested: (i) one CFS panel connected with two OSB panels, one on each side (labelled F-BSB), and (ii) one CFS panel connected with one OSB panel at its top (labelled as F-BS). For both specimens, the CFS and OSB panels were fastened with self-drilling screws at 100 mm intervals. Bare steel and OSB panels (labelled F-S and F-B, respectively) were also tested to provide a benchmark response. A summary of the specimens is presented in Table 1. The moisture content of three samples of OSB was measured using the oven dry method (BS EN 13183-2, 2007), giving a mean moisture content of 7.3%.

All specimens were simply supported on rollers and subjected to four-point bending. Two steel tubes, loaded by a spreader beam, were employed to distribute the load across the width of each specimen, at the positions of the point loads. Due to the slender nature of the CFS panel making it prone to local instabilities, and in line with EN 1993-1-3 (2006), the cross-sections of the specimens located at the positions of point loads and at the supports were locally strengthened with timber blocks to prevent premature localised failure of the CFS panel. A typical strengthened cross-section is shown in Figure 6. Vertical deflections at the positions of point loads and at mid-span were measured using linear variable displacement transducers (LVDTs) while the horizontal slip at the CFS-OSB interface was recorded at both ends of the composite panels using string potentiometers (SPs). The experimental setup is presented in Figure 7, while the cross-sections of the composite panels are shown in Figure 8.

It should be noted that there is no standardised testing method for bending tests on composite panels consisting of timber and steel. The loading rate used for structural testing of timber is usually higher than that used for steel. This is because a slow loading rate may lead to creep of timber whilst, for steel, a fast loading rate usually leads to overpredicted capacities and, thus, unconservative predictions for static load cases. Therefore, in order to examine the effect of the loading rate on the response of the OSB panels, trial tests were conducted with loading rates of 10 mm/min and 1.5 mm/min (i.e. approximately the maximum and minimum testing rates for timber specimens according to BS EN 12512 (2004)). Both rates were found to yield similar results and it was therefore concluded that both rates could be employed for the testing of the composite panels. Furthermore, although it is common practice for bending tests on steel members to involve several pauses of the displacement applied by the actuator for the determination of the actual moment capacity under static loading conditions (Huang and Young, 2013), the load on the OSB panels was observed to decrease rather than stabilise during such pauses. It was therefore decided that a constant displacement rate of 1.5 mm/min would be used for all specimens, with no pause of displacement during testing. In line with the standards for structural testing of timber products (EN 383, 2007) and in order to ensure settling in of the specimen and correct functioning of the instrumentation, the specimens comprising OSB panels (i.e. F-B, F-BS and F-BSB) were first loaded to approximately 40% of their peak load P_u, then unloaded to $0.1P_u$, and finally reloaded until failure. The loading procedure specified in EN 383 (2007) is shown in Figure 9.

3 RESULTS AND DISCUSSION

3.1 Material tests

3.1.1 Cold-formed steel

The measured and static stress-strain curves of a typical tensile coupon are shown in Figure 10. The static mechanical properties of all coupons, namely the Young's modulus E, yield strength f_y, ultimate strength f_u, strain at ultimate strength ε_u and fracture strain ε_f measured over the standard gauge length (BS ISO 6892-1, 2019) are summarised in Table 2. The mean measured yield strength of the steel material was found to be equal to 310.7 MPa, namely 11% higher than its nominal yield strength of 280 MPa.

3.1.2 OSB material

The stress-strain curves of two typical tensile and compressive OSB coupons are shown in Figure 11 and the mechanical properties obtained from the material tests are summarised in Table 3, where E_t and f_t are the Young's modulus and ultimate strength under tension and E_c

and f_c are the Young's modulus and ultimate strength under compression, respectively. The Young's modulus and ultimate strength under compression were found to be 10.9% and 14.5% higher than those corresponding to tension, respectively.

3.2 Push-out tests

As expected, all push-out specimens exhibited similar behaviour; the obtained load-slip responses are shown in Figure 12(a). The observed failure mode at the peak load of all specimens corresponded to shear failure of the connectors. However, significant bearing of the screws into the OSB panels had occurred prior to the peak load. A typical push-out specimen after failure is presented in Figure 12(b), where the deformed connectors can be seen. Note that in Figure 12(a), the loading - unloading cycles of all load-slip curves have been removed to allow direct comparison of the initial part of the responses of all specimens.

In line with EN 12512 (2004), the ductility of the connection D for each specimen was calculated according to Equation (1):

$$D = \frac{V_u}{V_y} \tag{1}$$

where V_u is the slip corresponding to 80% of the maximum load post-peak (for a slip of less than 30 mm) and V_y is the yield slip, determined as the slip at the intersection of the two tangents of the initial linear and latter nonlinear parts of the load-slip curve (EN 12512, 2004). A summary of the results is presented in Table 4, where $P_{c,u}$ is the maximum load per connector, s_u is the corresponding slip, K_o is the slip modulus of the connection calculated as the initial slope of the load-slip curve, K_1 is the average slope of load-slip curve during the unloading-reloading process, and D is the ductility of the connection.

3.3 Flexural tests

3.3.1 Test results

For all specimens comprising CFS sheeting (i.e. F-S, F-BS, F-SBS), failure was triggered due to local buckling developing between the point loads within the constant moment region – a typical example is shown in Figure 13. The load P carried by each flexural specimen is plotted against the midspan deflection δ_{mid} in Figure 14. As expected, for specimens F-BS and F-BSB, both the capacity and stiffness of the composite panel were substantially enhanced compared to the bare CFS panel (specimen F-S). The initial peak observed in the moment-curvature response of the composite specimens is attributed to the initiation of local buckling within the CFS sheeting. However, as also observed by Kyvelou *et al.* (2017a), due to the partial composite action present within the system, redistribution of internal forces permitted the system to carry more load.

The experimental results are summarised in Table 5 where M_u is the ultimate moment capacity of each specimen, $s_{h,u}$ is the recorded horizontal slip at ultimate load (averaged from measurements taken from both panel ends), δ_{mid} is the midspan deflection at maximum moment, EI is the flexural stiffness calculated based on the initial slope of load-midspan deflection curve according to Equation (2), and $(EI)_{loop}$ is the average flexural stiffness calculated at the unloading-reloading loops.

$$\delta_{mid} = \frac{P_1 a}{24EI}(3L^2 - 4a^2) \tag{2}$$

where P_1 is the load at each loading point (equal to $P/2$), a is the shear span (i.e. a = 0.5 m), and L is the length of the panel (i.e. L = 1.5 m).

In composite construction, the basic requirement for equally spaced shear connectors is sufficient deformation capacity in order for all connectors to be approximately equally loaded under flexure, allowing for sufficient redistribution of the longitudinal force at the shear interface (SCI, 2003; Johnson, 2004). Hence, the ductility of the shear connection employed in a composite system is important as it reflects its ability to undergo plastic deformations without a significant reduction in strength, allowing for redistribution within the system and preventing premature failure of the connection.

The results of the push-out tests showed that the connection employed between the CFS and OSB layers is sufficiently ductile such that, as reported in Table 4, an ultimate slip ranging from 10 mm to 13 mm can develop at the CFS-OSB interface. This ultimate slip is substantially larger than the equivalent peak slip recorded during the flexural tests (where the maximum recorded slip at the peak load of the system was 4.6 mm for specimen F-BSB) and, therefore, the connection is deemed capable of transferring the load effectively between the two materials up to failure. Thus, although splitting of the OSB panel and local buckling of the CFS sheet did occur for the composite panels (see Figure 15), they did not trigger brittle failure, as was the case for the non-composite specimens (i.e. F-S and F-B) – see Figure 16.

3.3.2 Comparison of response of composite panels with bare steel and non-composite panels

Comparisons between the ultimate moment capacity M_u and flexural stiffness EI of the composite specimens (i.e. F-BS and F-BSB) and those of the bare steel specimen (i.e. F-S) are presented in Figure 17(a) and Table 6. It is shown that when one OSB panel is employed, a 62% increase in moment capacity and 17% in flexural stiffness are achieved with screw spacing of 100 mm and steel wall thickness of 1.2 mm. Such results are generally consistent with the results reported by Kyvelou et al. (2017) for composite systems comprising cold-formed steel joist and wood-based floorboards connected with self-drilling screws. It was shown that the mobilisation of composite action led to 44.5% and 14.4% increase in moment capacity and flexural stiffness respectively for systems with screw spacing of 150 mm and steel wall thickness of 1.5 mm (Kyvelou et al., 2017).

For the system with two OSBs (one on top and one at the bottom of the CFS sheet – specimen F-BSB), increases of 84% and 23% in moment capacity and flexural stiffness are attained, respectively.

In order to present the benefits derived due to the mobilisation of composite action more clearly, the moment capacities M_u and flexural stiffnesses EI of all specimens, normalised by the capacity $M_{u,NC}$ and stiffness $(EI)_{NC}$ of the equivalent non-composite (NC) systems are presented in Figure 17(b). Note that the non-composite system NC corresponds to a system where both the CFS sheet and OSB panels are present and resist the applied bending, but are not connected and thus do not act as components of a composite system. Therefore, for the determination of the capacity and stiffness of the non-composite systems NC, it was assumed that the relative slip occurring at the CFS-OSB interface was free to develop (i.e. no connection between them). Hence, $(EI)_{NC}$ was calculated by summing the flexural stiffnesses of the bare CFS and OSB panels (i.e. $(EI)_{F\text{-}S}$ and $(EI)_{F\text{-}B}$, respectively) while $M_{u,NC}$ was determined as the sum of the ultimate capacity of the CFS panel $M_{u,F\text{-}S}$ and the moment attained by the OSB panel at a midspan deflection corresponding to $M_{u,F\text{-}S}$ (namely $M_{F\text{-}B}$ = 0.28 kNm). Hence, as reported in Table 6, an increase of 46% in strength and 9% in stiffness was achieved for specimen F-BS, while a 51% increase in strength and 7% in stiffness was attained by specimen F-BSB (relative to their equivalent non-composite systems).

3.4 Comparisons between test results and design predictions

In structural engineering, design standards are a well-established route to exploit new developments. Therefore, to facilitate the use of the proposed composite panels in the construction industry, design rules capable of predicting strength and stiffness of the proposed systems need to be established.

A design method devised by Kyvelou *et al*. (2017b) for the prediction of the moment capacity of composite cold-formed steel flooring systems has been employed to predict the capacity of the examined panels. According to Kyvelou *et al*. (2017b), the moment resistance of a composite panel $M_{c,Rd}$ ranges between the moment resistance of the bare CFS panel M_{CFS} (allowing for loss of effectiveness due to local instabilities) and the moment resistance of a fully composite panel $M_{pl,comp}$, depending on the degree of shear connection η – see Figure 18. The moment resistance $M_{u,Rd}$ can be calculated according to Equation (3), where $M_{pl,Rd}$ is the moment capacity of a panel with the same degree of partial shear connection as the examined system, derived based on the equilibrium method of EN 1994-1-1 (2005), assuming a plastic distribution of stresses.

$$M_{u,Rd} = M_{pl,Rd} - (1 - \eta)\,(M_{pl,CFS} - M_{CFS}) \tag{3}$$

$$\eta = \frac{n}{n_f} \leq 1 \tag{4}$$

In Equation (4), n is the number of connectors in the critical lengths of the examined panel and n_f is the number of connectors that would be required for the development of full shear connection at the CFS-OSB interface.

Comparisons between the ultimate moment capacities $M_{u,Rd}$ predicted by this design method and those obtained from the physical tests are presented in Table 7. Note that for the unfavourable load case of uplift loading where the CFS sheet would be subjected to compression and the OSB panel to tension, in line with the recommendations provided by Kyvelou *et al*. (2017b), no composite action can be assumed and the moment capacity $M_{u,Rd}$

shall be taken equal to the moment capacity of the equivalent non-composite system, as described in Section 3.3.2.

For the calculation of the effective flexural stiffness of the examined composite panels $(EI)_{\mathrm{eff}}$, a method described in Section B.2 of Annex B of EN 1995-1-1 (2004) for mechanically jointed beams has been employed; this has been derived analytically, based on fundamental mechanics (Kreuzinger, 1995). According to this method, which is a modified version of the parallel axis theorem, the effective flexural stiffness of $(EI)_{\mathrm{eff}}$ can be calculated according to Equation (5).

$$(EI)_{\mathrm{eff}} = \sum_{i=1}^{3} \left(E_{\mathrm{i}} I_{\mathrm{i}} + \gamma_{\mathrm{i}} E_{\mathrm{i}} A_{\mathrm{i}} a_{\mathrm{i}}^{2} \right) \tag{5}$$

In Equation (5), E_{i}, A_{i} and I_{i} are the Young's modulus, cross-sectional area and second moment of area of each component respectively, a_{i} is the distance between the neutral axes of each component and that of the whole cross-section and γ_{i} is a coefficient allowing for the influence of the slip at the shear interface, which can be calculated according to Equation (6):

$$\gamma_{\mathrm{i}} = \left[1 + \pi^{2} E_{\mathrm{i}} A_{\mathrm{i}} s_{\mathrm{i}} / \left(K_{\mathrm{i}} l^{2} \right) \right]^{-1} \tag{6}$$

where L is the span, s_{i} is the spacing of the fasteners and K_{i} is the slip modulus of the employed connection (herein determined by the conducted push-out tests – see Table 4). A schematic illustration of the section dimensions is presented in Figure 19. Comparisons between the effective flexural stiffnesses $(EI)_{\mathrm{eff}}$ predicted by the employed design method and those obtained from the physical tests EI are presented in Table 7.

It should be mentioned that, although further test results would be required to fully validate these theoretical methods, reasonable agreement was found between the design predictions and the experimental results, with the design predictions being on the conservative side.

4 CONCLUSIONS

An experimental programme has been carried out to investigate the composite behaviour of panels comprising cold-formed steel sheeting and oriented strand boards, connected with self-drilling screws. A series of material, push-out and flexural tests was performed to explore the structural behaviour of the proposed system as well as of its constituent components.

Flexural tests on full-scale panels demonstrated that the mobilisation of composite action through the use of a substantial shear connection (self-drilling screws at 100 mm spacing) is feasible, leading to up to 10% and 50% increases in flexural stiffness and moment capacity for the examined systems respectively, improving their performance both under serviceability and ultimate limit states. The significant increases in moment capacity and stiffness could translate to significant material savings when compared to equivalent systems without the effect of composite action. Weight savings increase the suitability of the proposed panel system for use in earthquake-prone regions, as well as improving panel handling for manual construction in rapidly developing or informal settlements. The exact suitability of this system for resisting seismic loading is a topic of ongoing research.

Existing design rules were found to generally provide conservative predictions of the moment capacity and flexural stiffness of these panels. Ongoing research comprises further physical tests and the development of finite element models that, after validation, will allow the influence of further key parameters to be examined. Ultimately, the establishment of reliable design rules harnessing the beneficial influence of composite action for the proposed panels is envisaged in order to promote their use in practice.

ACKNOWLEDGEMENETS

The EPSRC GCRF Institutional Sponsorship Award from the University of Edinburgh funded this work. The authors are grateful to the exchange PhD student Ms Zixuan Chen, funded by the Chinese Scholarship Council, for her assistance in the experimental programme. The authors would like to thank Dr Vasdravellis for providing lab access at Heriot Watt University. The authors would also like to thank Mr Noueihed Karim for his work in analysing the test results, as part of his British Council IAESTE internship programme.

REFERENCES

BS EN 10326. (2004) *Continuously hot-dip coated strip and sheet of structural steels. Technical delivery conditions*. British Standard Institution (BSI), London.

BS EN 789. (2004) *Timber Structures. Test Methods. Determination of mechanical properties of wood-based panels*. British Standard Institution (BSI), London.

BS EN 13183-2. (2007) *Moisture content of a piece of sawn timber - Part 1: Determination by the oven dry method*. Brussels: European Committee for Standardization.

BS ISO 6892-1. (2019) *Metallic Materials. Tensile Testing. Method of test at room temperature*. British Standard Institution (BSI), London.

Chopra A.K. (2020) *Dynamics of Structures: Theory and Applications to Earthquake Engineering*. (5th edition). Harlow, England: Pearson.

EN 12512. (2004) *Timber structures - Test methods – Cyclic testing of joints made with mechanical fasteners*. Brussels: European Committee for Standardization.

EN 1993-1-3. (2006) *Design of steel structures - Part 1-3: General rules - Supplementary rules for cold-formed members and sheeting*. Brussels: European Committee for Standardization.

EN 1994-1-1. (2005) *Eurocode 4. Design of composite steel and concrete structures. General rules and rules for buildings*. Brussels: European Committee for Standardization.

EN 1995-1-1. (2004) *Eurocode 5. Design of timber structures. Part 1-1: General — Common rules and rules for buildings*. Brussels: European Committee for Standardization.

EN 383. (2007) *Timber structures. Test methods. Determination of embedment strength and foundation values for dowel type fasteners*. Brussels: European Committee for Standardization.

Fratamico D.C., Torabian S., Zhao X., Rasmussen K.J.R. and Schafer B.W. (2018) Experimental study on the composite action in sheathed and bare built-up cold-formed steel columns. *Thin-Walled Structures*, 127, 290-305.

Johnson R.P. (2004) *Composite structures of steel and concrete. Beams, slabs, columns, and frames for buildings*. Third ed., Blackwell Publishing.

Henriques J., Rosa N., Gervasio H., Santos P. and Simoes da Silva L. (2017) Structural performance of light steel framing panels using screw connections subjected to lateral loading. *Thin-Walled Structures*, 121, 67-88.

Huang Y. and Young B. (2013) Experimental and numerical investigation of cold-formed lean duplex stainless steel flexural members. *Thin-Walled Structures*, 73, 216-228.

Huang Y. and Young B. (2014) The art of coupon tests. *Journal of Constructional Steel Research*, 96, 159-175.

Karki D., Far H. and Saleh A. (2021) Numerical studies into factors affecting structural behaviour of composite cold-formed steel and timber flooring systems. *Journal of Building Engineering*, 44, 102692.

Kreuzinger H. (1995) Mechanically jointed beams and columns. In: Blass HJ, Aune P, Choo BS, Gorlacher R, Griffiths DR, Hilson BO et al. (Eds.), *Timber Engineering. STEP 1. Basis of design, material properties, structural components and joints*. Centrum Hout, The Netherlands.

Kyprianou C., Kyvelou P., Gardner L. and Nethercot D.A. (2018) Numerical study of sheathed cold-formed steel columns. In: *Proceedings of the 9th International Conference on Advances in Steel Structures (ICASS'2018)*, 5-7 December, Hong Kong, China.

Kyvelou P., Gardner L. and Nethercot D.A. (2015) Composite action between cold-formed steel beams and wood-based floorboards. *International Journal of Structural Stability and Dynamics*, 15(8), 1540029.

Kyvelou P., Gardner L. and Nethercot D.A. (2017) Testing and Analysis of Composite Cold-Formed steel and Wood-Based Flooring Systems. *Journal of Structural Engineering*, 143(11), 04017146.

Kyvelou P., Gardner L. and Nethercot D.A. (2017) Design of Composite Cold-Formed Steel Flooring Systems. *Structures*, 12(1), 242-252.

Kyvelou P., Gardner L. and Nethercot D.A. (2018) Finite Element Modelling of Composite Cold-Formed Steel Flooring Systems. *Engineering Structures*, 158(1), 28-42.

Li X. (2005) *Composite beams of cold-formed steel sections and wood members*. PhD Thesis, The University of New Brunswick, Canada.

Loss C. and Frangi A. (2017) Experimental investigation on in-plane stiffness and strength of innovative steel-timber hybrid floor diaphragms. *Engineering Structures*, 138, 229-244.

Navaratnam S., Widdowfield Small D., Gatheeshgar P., Poologanathan K., Thamboo J., Higgins C. and Mendis P. (2021) Development of cross laminated timber-cold-formed steel composite beam for floor system to sustainable modular building construction. *Structures*, 32, 681-690.

Rahman S., de Groot W.T. and Snelder D.J. (2008) Exploring the Agroforestry Adoption Gap: Financial and Socioeconomics of Litchi-Based Agroforestry by Smallholders in Rajshahi (Bangladesh). *Smallholder Tree Growing for Rural Development and Environmental Services: Lessons From Asia*, 5, 227-243.

Schafer BW. (2011) Cold-formed steel structures around the world. *Steel Construction*, 4(3), 141-149.

SCI. (2003) *Shear connection in composite beams*, Advisory Desk, AD 266.

UN Habitat. (2020) *World Cities Report 2020: The Value of Sustainable Urbanization*. [online] Available from: https://unhabitat.org/World%20Cities%20Report%202020.

Vella N., Gardner L. and Buhagiar S. (2020) Experimental analysis of cold-formed steel-to-timber connections with inclined screws. *Structures*, 24, 890-904.

Table 1: *Description of tested flexural specimens*

Specimen	Description	Connectors
F-S	Bare CFS	NA
F-B	Bare OSB	NA
F-BS	OSB- CFS	Self-drilling screws
F-SBS	OSB-CFS-OSB	Self-drilling screws

Table 2: *Static mechanical properties of cold-formed steel coupons*

Coupon	E (MPa)	f_y (MPa)	f_u (MPa)	ε_u (%)	ε_f (%)
1	202300	312.7	382.2	20.8	27.3
2	200100	308.5	383.0	20.9	24.3
3	202300	310.8	396.6	---	---
MEAN	**201600**	**310.7**	**387.4**	**20.9**	**25.8**

Table 3: *Mechanical properties of OSB material*

	Compression		Tension	
Coupon	E_c (MPa)	f_c (MPa)	E_t (MPa)	f_t (MPa)
1	3685	11.02	3918	10.35
2	4374	11.81	3454	9.94
3	4206	11.99	- (clamp failure)	- (clamp failure)
MEAN	**4088**	**11.61**	**3686**	**10.14**

Table 4: *Summary of results obtained from push-out tests*

Specimen	$P_{c,u}$ (kN)	s_u (mm)	K_o (N/mm)	K_l (N/mm)	D
1	2.23	10.6	428	N/A	3.1
2	2.34	13.0	325	1271	4.0
3	2.28	14.3	297	1955	3.3
AVERAGE	**2.29**	**12.6**	**350**	**1613**	**3.5**

Table 5: *Results of flexural tests*

Specimen	M_u (kNm)	$s_{h,u}$ (mm)	δ_{mid} (mm)	EI (Nm^2)	$(EI)_{loop}$ (Nm^2)
F-S	2.51	NA	30.9	30430	NA
F-B	0.83	NA	105.9	2314	2363
F-BS	4.07	1.8	43.4	35662	51673
F-BSB	4.62	4.6	73.4	37555	49697

Table 6: *Comparison of moment capacity and flexural stiffness of composite panels to equivalent non-composite and bare steel specimens*

Specimen	$M_u/M_{u,F\text{-}S}$	$EI/(EI)_{F\text{-}S}$	Specimen	$M_u/M_{u,NC}$	$EI/(EI)_{NC}$
F-S	1.00	1.00	NC	1.00	1.00
F-BS	1.62	1.17	F-BS	1.46	1.09
F-BSB	1.84	1.23	F-BSB	1.51	1.07

Table 7: *Comparison between test results and design predictions of moment capacity and flexural stiffness of composite panels*

Specimen	$M_u/M_{u,Rd}$	$EI/(EI)_{eff}$
F-BS	1.26	1.29
F-BSB	1.04	1.28

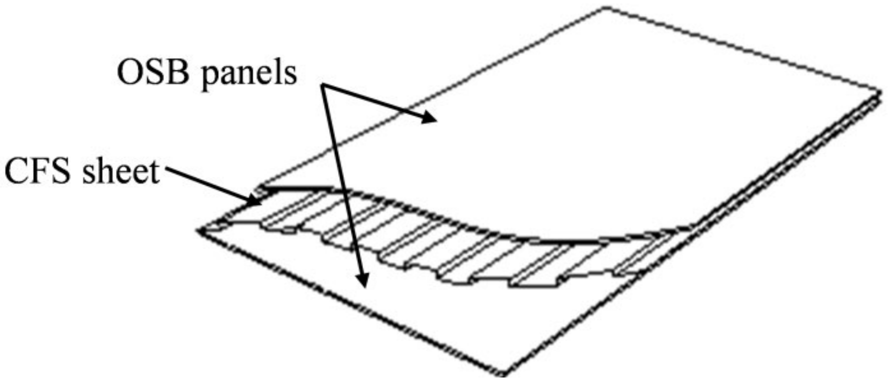

Figure 1: *Illustration of the proposed panel*

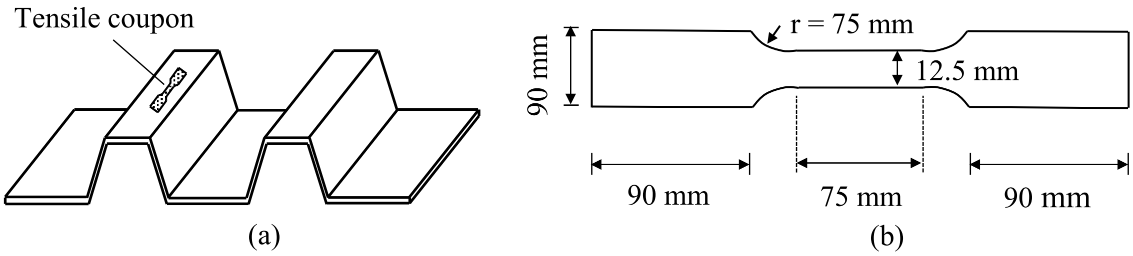

Figure 2: *(a) Position and (b) dimensions of CFS coupons*

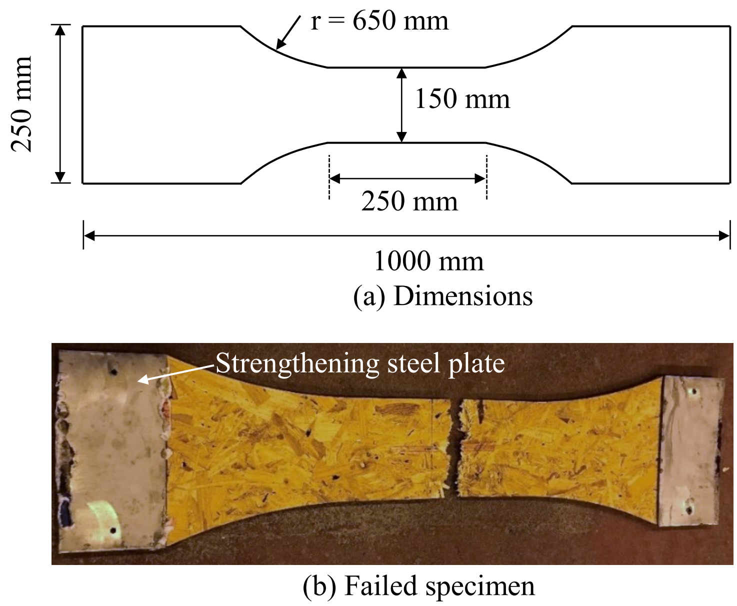

Figure 3: *OSB tensile specimen*

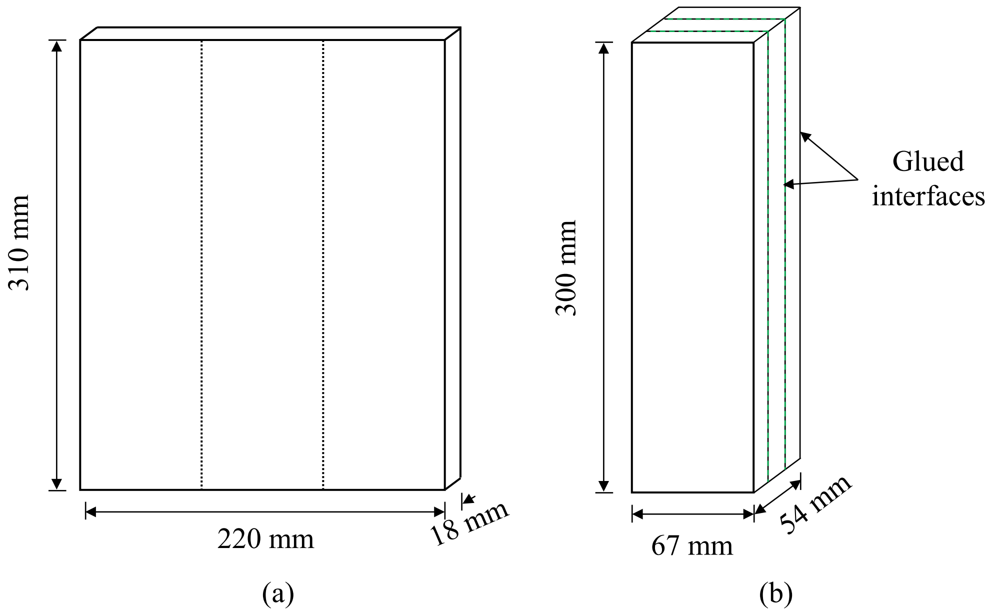

Figure 4: Dimensions of (a) test piece and (b) final compressive coupon from OSB panel

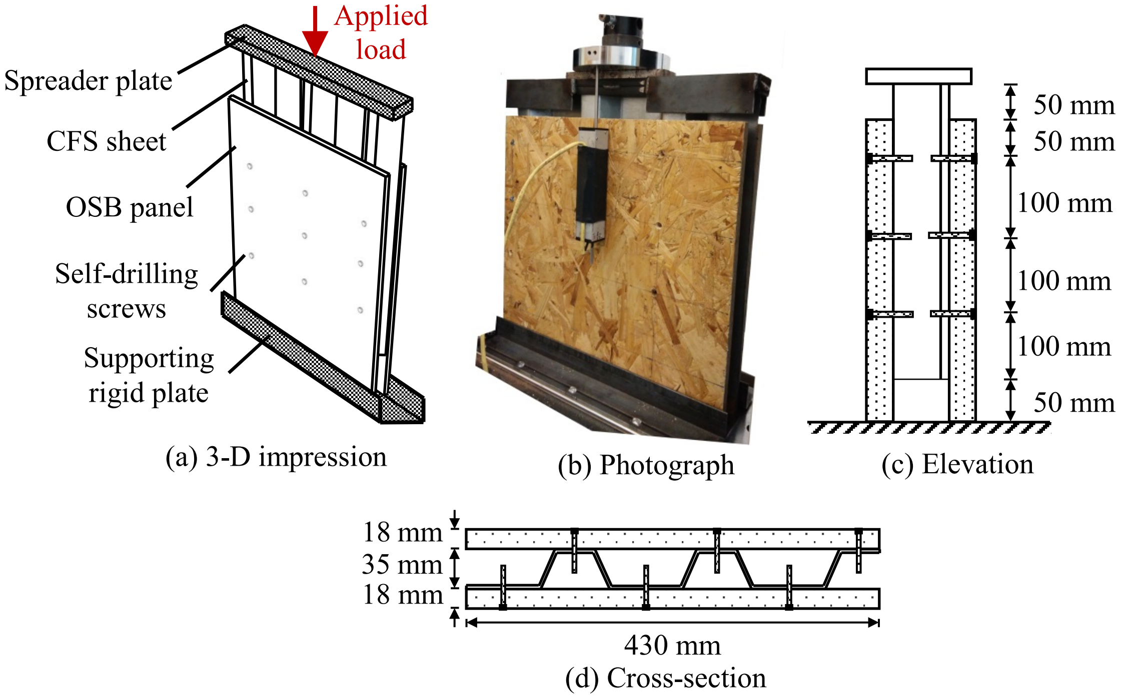

Figure 5: *(a) 3-D impression, (b) photograph, (c) elevation and (d) cross-section of typical push-out specimen*

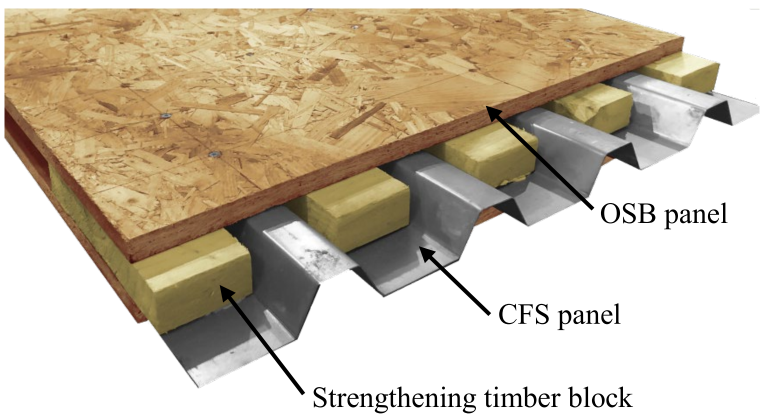

Figure 6: *Strengthened cross-section at the positions of point loads and supports*

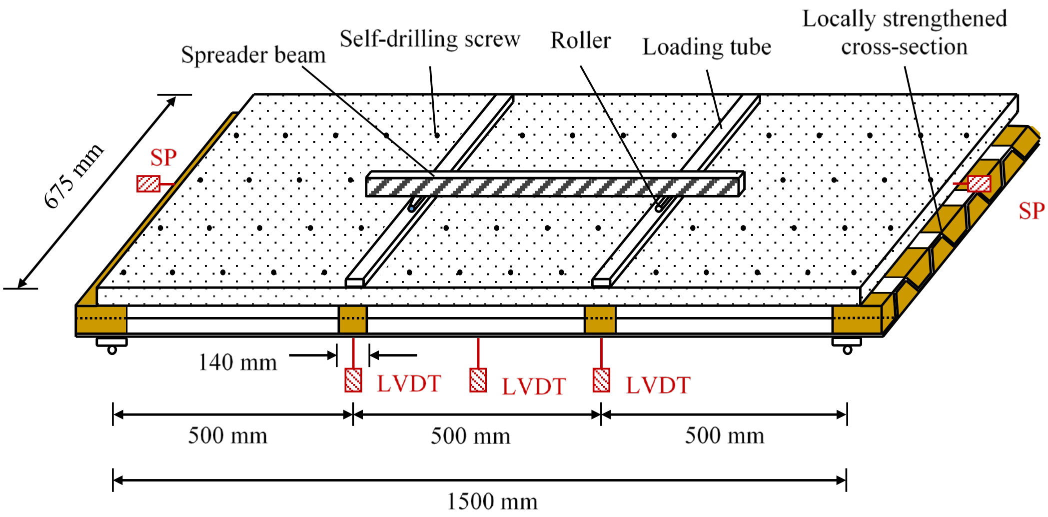

(a) Schematic illustration

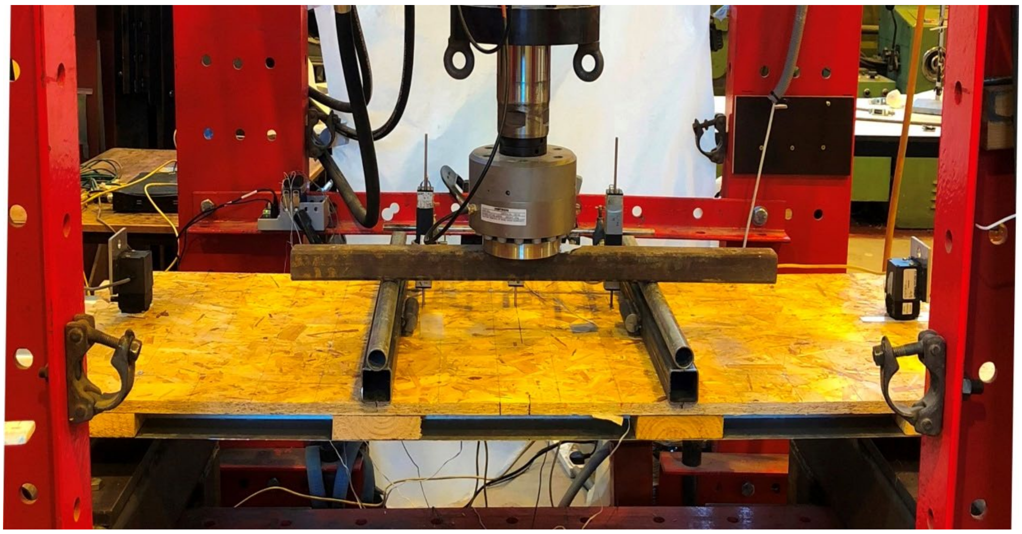

(b) Photograph

Figure 7: *(a) Schematic illustration and (b) photograph of experimental layout and instrumentation of flexural tests (shown for specimen F-BS)*

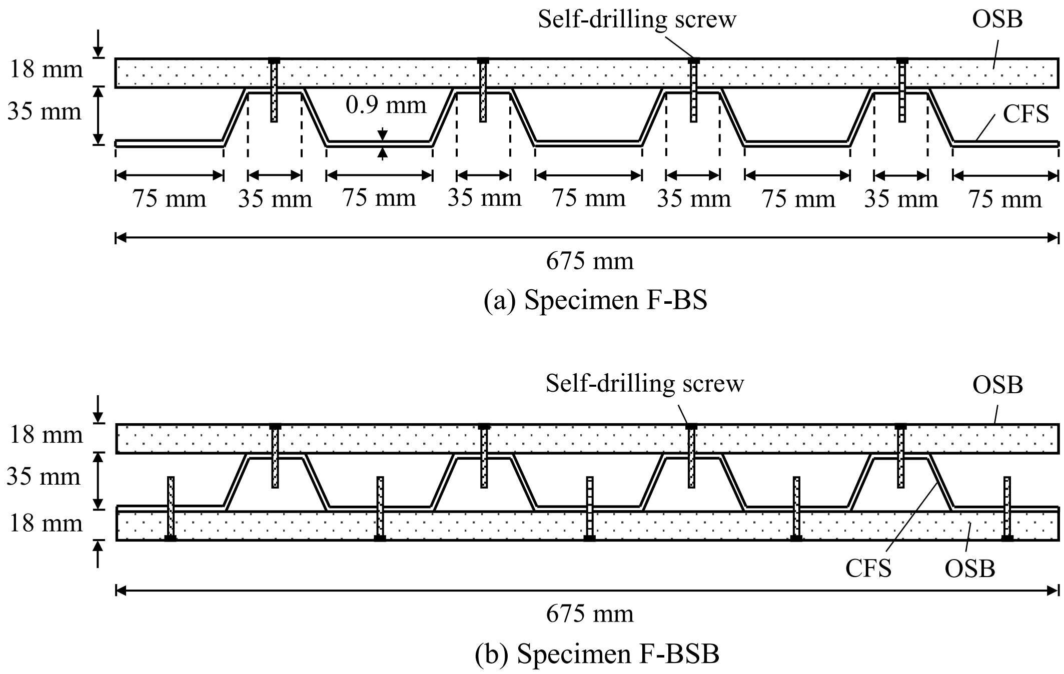

Figure 8: *Cross-sections of tested composite panels*

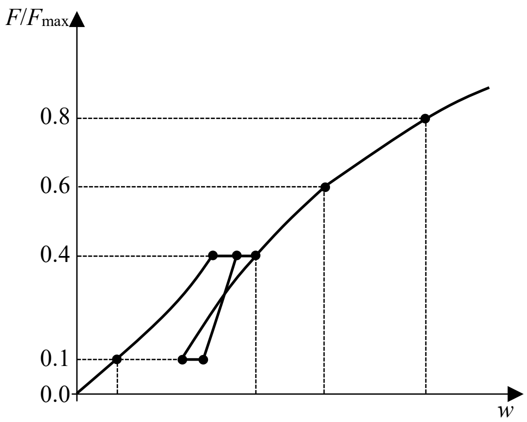

Figure 9: *Idealised load-deformation curve of the testing procedure recommended by EN 383 (2007)*

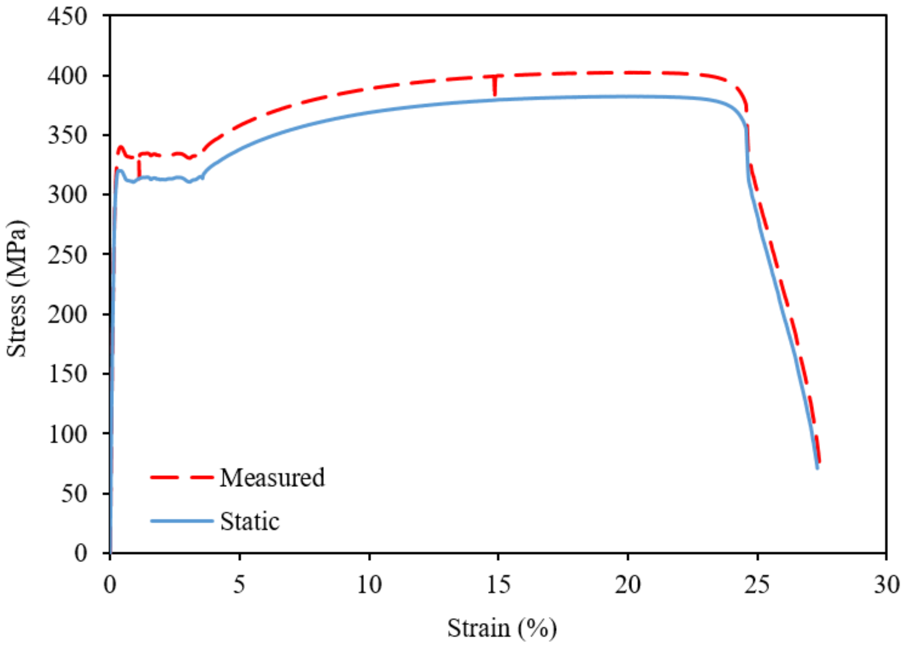

Figure 10: *Stress-strain curve of typical cold-formed steel tensile coupon*

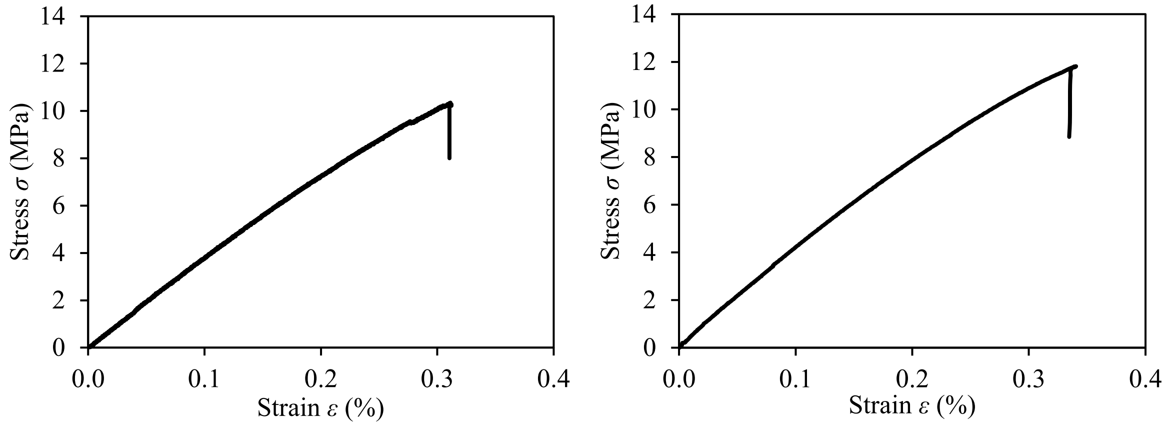

(a) Tension

(b) Compression

Figure 11: *Typical stress-strain curve of OSB coupon under: (a) tension and (b) compression*

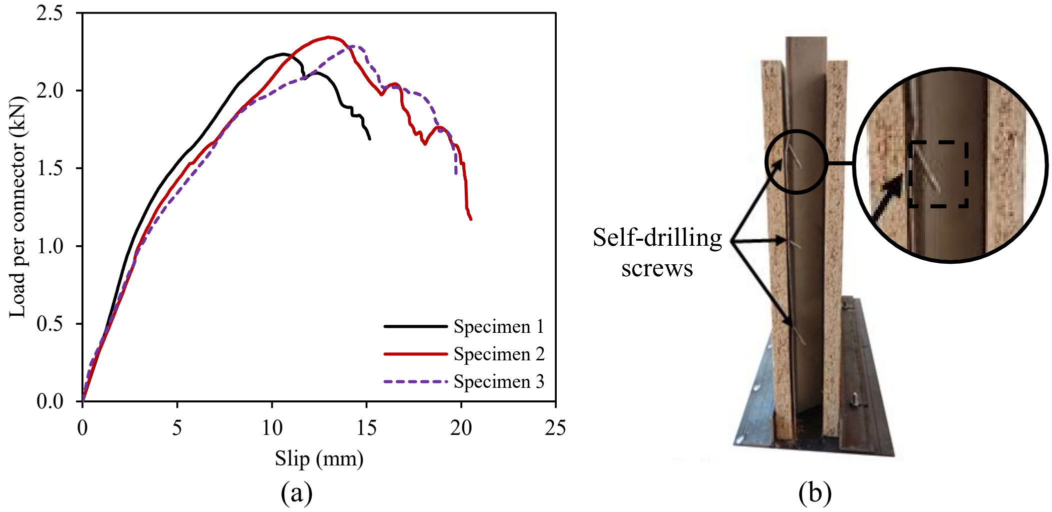

Figure 12: *Push-out specimens: (a) load-slip responses and (b) typical failure mode*

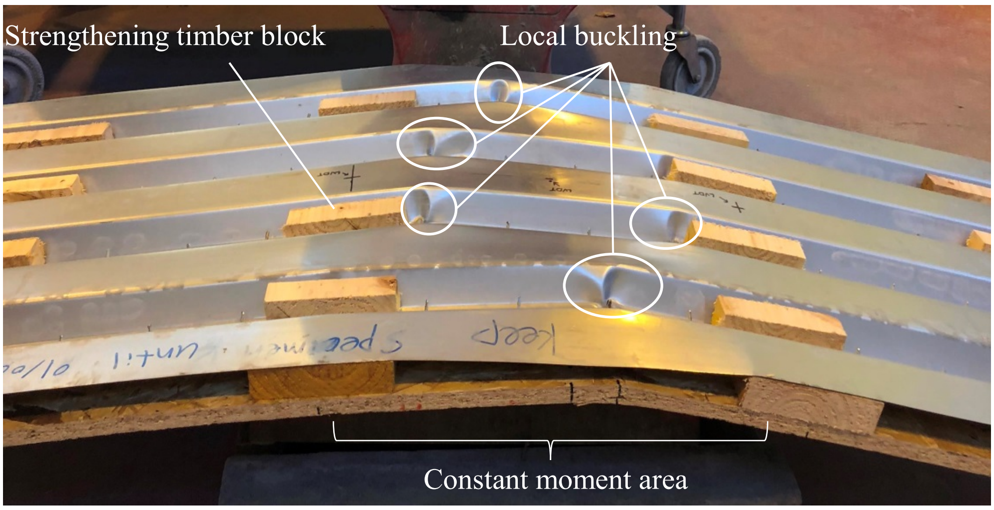

Figure 13: *Local buckling at peak load of specimen F-BS (figure shows specimen underside)*

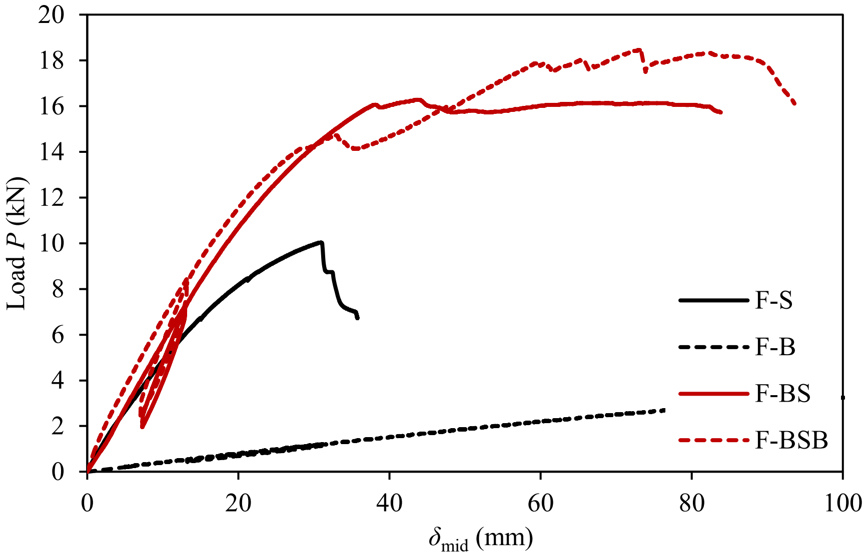

Figure 14: *Load-midspan deflection curves*

Figure 15: *Deformed shape of composite panel (specimen F-BSB)*

(a) Specimen F-B

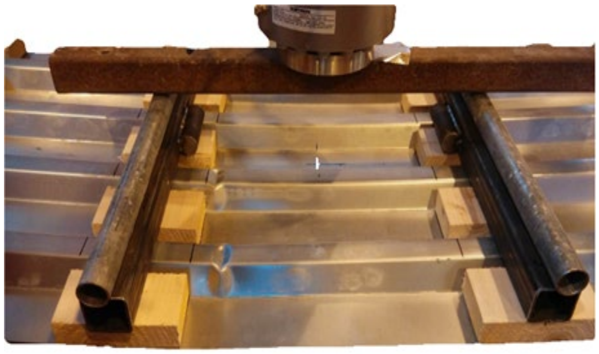

(b) Specimen F-S

Figure 16: *Failure modes of non-composite specimens*

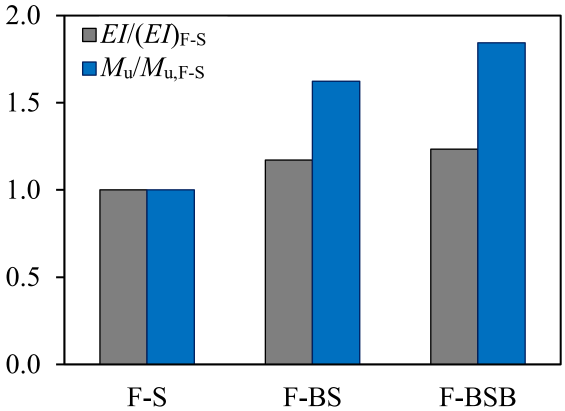

(a)

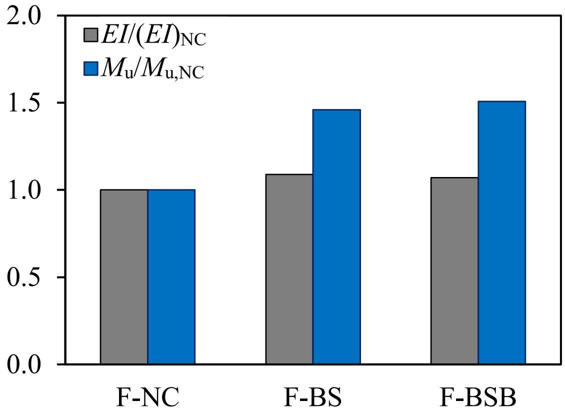

(b)

Figure 17: *Improvements in terms of moment resistance and flexural stiffness of composite specimens compared to equivalent (a) bare steel and (b) non composite systems*

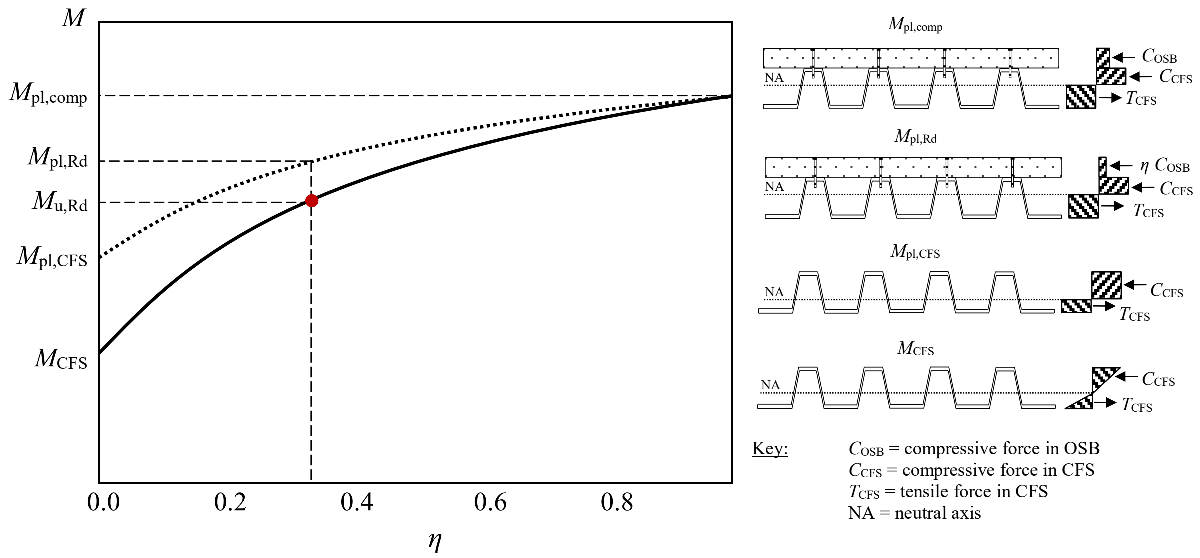

Figure 18: *Moment capacities required for the calculation of the moment resistance of the composite panel $M_{c,Rd}$*

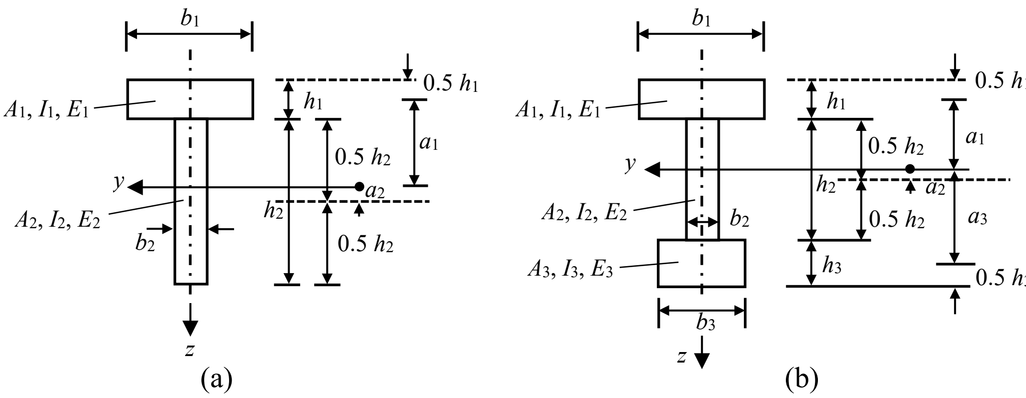

Figure 19: *Dimensions used for the calculation of the effective stiffness of composite beam comprising: (a) two laminates and (b) three laminates (EN 1995-1-1, 2004)*